Balkan Journal of Electrical and Computer Engineering (BAJECE)
Volume 1 Number 1, September 2023

African Vultures Optimization Algorithm-Based Selective Harmonic Elimination for Multi-level Inverter

Yasin Bektas

1 Department of Electrical-Electronic Engineering Aksaray University, Aksaray, Turkey,(e-mail: yasinbektas@aksaray.edu.tr)

Manuscript received Apr 10, 2023; accepted August 26, 2023.

***Abstract*—In recent years, multilevel inverters have gained significant attention due to their advantages, such as improved output waveform quality and reduced harmonic distortion. However, harmonics in multilevel inverter systems continue to be a persistent issue. Researchers have addressed this problem using the Selective Harmonic Elimination-Pulse Width Modulation (SHE-PWM) technique. However, the SHE equations formulated for eliminating or reducing the selected harmonics involve complex and computationally intensive calculations, encompassing nonlinear and transcendental equations. Various optimization techniques have been developed to tackle these intricate and demanding calculations. This article presents a new approach that utilizes the relatively newly developed African Vultures Optimization (AVO) algorithm to solve the SHE equations in multilevel inverters. The AVO-based SHE-PWM technique is tested on a three-phase cascade multilevel inverter (CHB-MLI) with 7, and 11 levels. The proposed algorithm demonstrates the ability to locate adequate solutions within the modulation index range of 0.1 to 1.0. It is shown that the modulation index range of 0.5 to 1.0 allows for the successful elimination of the selected harmonics and precise control of the fundamental voltage with an error of less than 0.5%.**

Index Terms—**African Vultures Optimization Algorithm, Multi-level inverter, Selective Harmonic Elimination, Optimization.**

I. Introduction

Multilevel inverters find applications in various fields, including renewable energy systems (such as solar and wind energy integration), electric vehicles, high-voltage direct current (HVDC) transmission systems, and medium-voltage motor drives [1-6]. Their ability to generate high-quality output waveforms makes them suitable for applications that require solid power quality. Alongside the circuit structures of multilevel inverters, control techniques play a crucial role. Among the most popular modulation techniques used for multilevel inverters are pulse width modulation (PWM), selective Harmonic elimination (SHE-PWM), and space vector PWM (SV-PWM) [7-9]. These techniques enhance the efficiency of the inverter while also lowering the amount of harmonic distortion that is present in the waveform that is produced. SHE-PWM stands out as the most effective due to its direct harmonic elimination capability. SHE-PWM is a modulation technique that selectively eliminates or reduces lower-order harmonics in the output waveform. When SHE-PWM is used, the output waveform is improved with smoother characteristics, and the total harmonic distortion (THD) value is reduced. This minimizes the effect of unwanted harmonic components and yields a cleaner output waveform.

Various optimization methods have been developed to address the computational complexity of SHE. These optimization techniques aim to find optimum switching angles that satisfy the desired harmonic elimination conditions while minimizing the computational effort. Genetic Algorithms (GA) [10], Particle Swarm Optimization (PSO) [11], Differential Evolution (DE) [12], Artificial Bee Colony (ABC) [13], Red Deer Algorithm (RDA) [14], and other metaheuristic algorithms have been applied in SHE optimization. These algorithms explore the solution space to find the best solutions, considering factors such as convergence speed, computational efficiency, robustness, and the ability to handle different modulation indices. Utilizing optimization methods in selective harmonic elimination enables the efficient implementation of multilevel inverters, achieves high-quality output waveforms, and reduces harmonic distortion. Researchers and engineers can adapt the performance of multilevel inverters to meet specific application requirements, optimize power conversion efficiency, and adhere to power quality standards by selecting an appropriate optimization algorithm. Ongoing research in this field aims to enhance the efficiency and accuracy of optimization algorithms and their application in real-time control systems, thus paving the way for the widespread adoption of multilevel inverters in various power electronics applications.

This study presents a new approach that utilizes the African Vultures Optimization (AVO) algorithm [15] to solve the SHE equations in multilevel inverters. The results show that the proposed algorithm works well at finding reasonable solutions within a specific range of modulation indices, allowing the elimination of certain harmonics and precise control of the fundamental voltage. This research contributes to the

advancement of optimization techniques in multilevel inverters and offers promising possibilities for improving power quality in various applications.

II. Material And Method

A. *Cascaded Multilevel Inverters*

Multilevel inverters come in three main topologies: diode-clamped, capacitor-clamped, and cascaded. Among these structures, cascade multi-level inverter has different advantages compared to other inverter types. The cascaded H-bridge inverter (CHB) structure with distinct DC sources is the topology that needs the fewest number of components overall. Because of its modular design and flexible circuit configuration, it is well suited for use in applications requiring high voltage and high power. A cascaded H-bridge multilevel inverter, also known as a CHB-MLI, is created by joining a number of single-phase H-bridge inverters in a series configuration, as seen in Fig. 1(a) for an N-level inverter. N=2m+1 describes how many different levels of output phase voltage the CHB-MLI can produce, where m refers to the number of H-bridges used in each phase. Each H-bridge is fed by its own individual DC source. The three distinct voltage levels of $+V_{DC}$, 0 V_{DC}, and $-V_{DC}$ may be achieved by choosing various combinations of the switches labelled S_1, S_2, S_3, and S_4 located inside each H-bridge. In order to make the synthesized AC voltage waveform identical to the sum of all the voltages produced by the cascaded H-bridge cells, the outputs of the H-bridge switches are connected in series with one another.

Depending on the application, a three-phase circuit structure is obtained by either star or delta connection. This study uses three-phase circuit structures with 7, and 11 levels. For seven levels, three H-bridge structures are required for each phase, while four H-bridge structures are needed for nine levels, and five H-bridge structures are required for eleven levels.

B. *Mathematical Model of SHE-PWM Technique*

Selective Harmonic Elimination (SHE) is a PWM (pulse width modulation) technique commonly used at low frequencies. Its purpose is to control the output voltage while adjusting the fundamental harmonic to the desired value and eliminating selected harmonics to achieve a sinusoidal AC output voltage waveform. After applying SHE-PWM, the remaining insignificant higher-order harmonics can be eliminated using a small passive filter. In the SHE-PWM technique, a set of nonlinear equations, usually denoted by m, is solved to find the optimum switching angles for different modulation indices.

One of the equations equals the fundamental harmonic value, while the others are set to zero to eliminate the selected harmonics. Subsequently, the switching angles that satisfy these equations are calculated using appropriate methods. The nonlinear harmonic equations required to obtain the optimal switching angles can be expressed using the Fourier series expansion of the output voltage. The expression for the output voltage, which includes all harmonic components, can be defined as shown in Eq. (1).

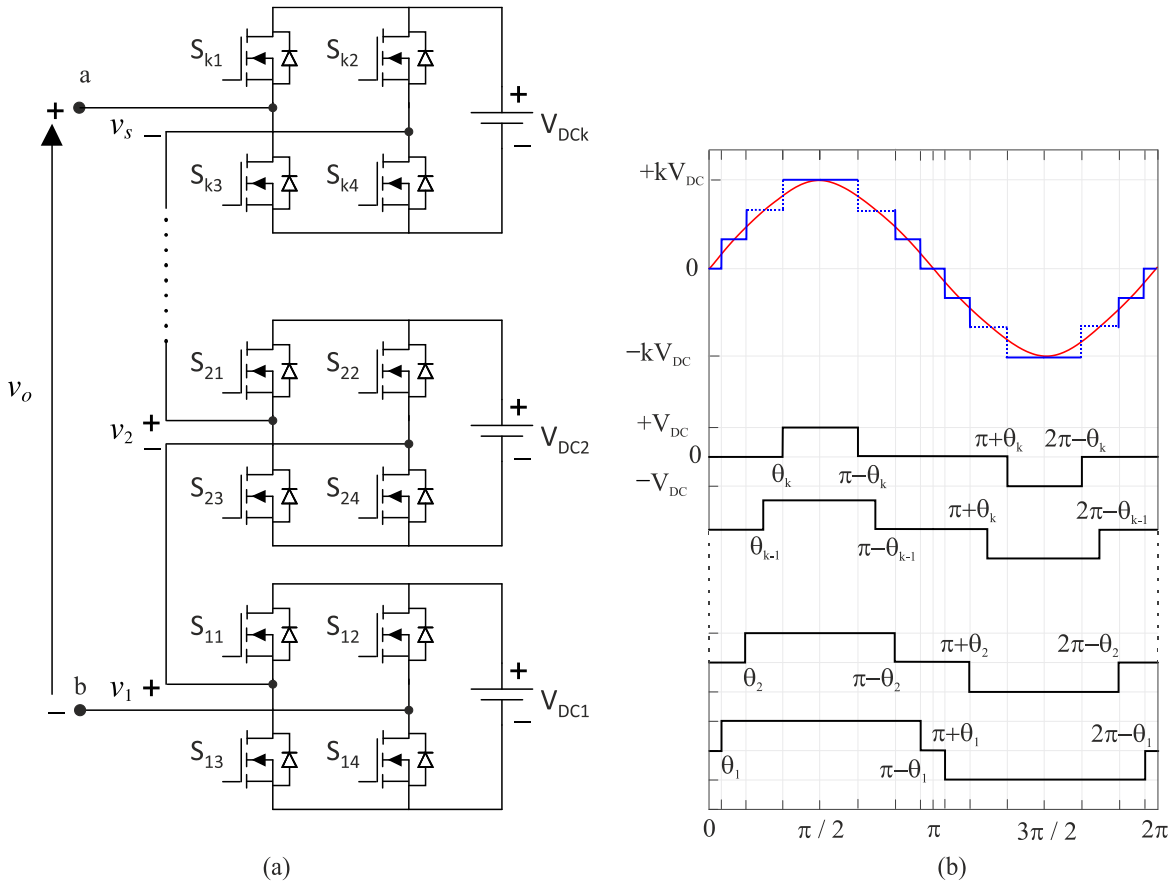

Fig.1. Single-phase N-level CHB-MLI (a) circuit structure (b) output voltage waveform

$$V_{ab}(\omega t)=\sum_{n=1,3,5,7,\ldots}^{\infty}\frac{4V_{DC}}{n.\pi}*[\cos(n\theta_1)+\cos(n\theta_2)+\cdots+\cos(n\theta_{k-1})+\cos(n\theta_k)]*[\sin(nwt)] \quad (1)$$

where, V_{DC} is the input voltage for each H-bridge inverter. θ_1, θ_2, ..., and θ_k are the switching angles, and due to quarter-wave symmetry, the switching angles should satisfy the condition in Eq.(2).

$$0\le\theta_1<\theta_2<\ldots<\theta_{k-1}<\theta_k\le\frac{\pi}{2} \quad (2)$$

k represents the number of switching angles, and n represents the degree of the harmonic. For the 7-level, and 11-level inverters, the required number of discrete DC sources is three, four, and five, respectively. In a balanced three-phase system, there are no harmonics that are multiples of three, so the harmonics that are multiples of three are not considered. Typically, in the context of *k* switching angles, a single switching angle is employed to regulate the intended fundamental output voltage V_1, while the remaining (*k*-1) switching angles are utilised to elimination or diminish the low-order harmonics (*k*-1). The Eq.(1) provides the formula for the fundamental output voltage V1, expressed in relation to the switching angles.

$$V_1=\frac{4V_{DA}}{\pi}\left(\cos(\theta_1)+\cos(\theta_2)+\cdots+\cos(\theta_{k-1})+\cos(\theta_k)\right) \quad (3)$$

The modulation index controls the fundamental voltage in the SHE technique. M, can be defined as the ratio of the peak value (V1p) of the desired base voltage given in (4) to the total DC input voltage [16].

$$M=\frac{V_{1p}}{kV_{DA}} \quad (4)$$

The determination of the modulation index and switching angles that result in the generation of an AC waveform with minimal total harmonic distortion (THD) necessitates the resolution of k transcendental nonlinear equations, commonly referred to as SHE equations, that describe the chosen harmonics.

The seven-level inverter utilizes three h-bridge structures. The SHE equations for the 7-level inverter are as follows:

$$\begin{aligned}V_1&=\cos(\theta_1)+\cos(\theta_2)+\cos(\theta_3)=Mk\,\pi/4\\V_5&=\cos(5\theta_1)+\cos(5\theta_2)+\cos(5\theta_3)=0\\V_7&=\cos(7\theta_1)+\cos(7\theta_2)+\cos(7\theta_3)=0\end{aligned} \quad (5)$$

The eleven-level inverter utilizes five h-bridge structures. The SHE equations for the 11-level inverter are as follows:

$$\begin{aligned} V_1 &= \cos(\theta_1) + \cos(\theta_2) + \ldots + \cos(\theta_5) = Mk\,\pi/4 \\ V_5 &= \cos(5\theta_1) + \cos(5\theta_2) + \ldots + \cos(5\theta_5) = 0 \\ V_7 &= \cos(7\theta_1) + \cos(7\theta_2) + \ldots + \cos(7\theta_5) = 0 \\ V_{11} &= \cos(11\theta_1) + \cos(11\theta_2) + \ldots + \cos(11\theta_5) = 0 \\ V_{13} &= \cos(13\theta_1) + \cos(13\theta_2) + \ldots + \cos(13\theta_5) = 0 \end{aligned} \quad (6)$$

For the correct solution, the switching angles for all inverter states must satisfy the condition $0 \le \theta_1 < \theta_2 < \ldots \le \theta_k$. In this study, two different total harmonic distortion values will be calculated. The first is %THD, and the other is % THDe. The %THD limit value is usually infinite but will be considered up to the 50th harmonic. THDe represents the total value of the harmonics to be eliminated. When calculating the THDe [16] value, the maximum harmonic value to be eliminated is considered. The maximum harmonic value for the seven-level is 7th, 11th , and 13thfor the eleven-level.

$$\%THD = \frac{\sqrt{V_5^2 + V_7^2 + V_{11}^2 + \cdots V_{49}^2}}{|V_1|} \quad (7)$$

$$\%THD_e = \frac{\sqrt{V_5^2 + V_7^2 + \ldots}}{|V_1|} \quad (8)$$

C. African Vultures Optimization Algorithm

African Vulture Optimization (AVO) is an optimization algorithm developed by drawing inspiration from the feeding behavior of vultures in natural habitats. Vultures efficiently locate their prey over a wide area through their social interactions and observational abilities. Mimicking these natural strategies, the AVO algorithm is used to solve complex optimization problems. It employs a population-based approach and utilizes a set of candidate solutions (individuals) to solve the problem. The algorithm moves each individual through steps that imitate the vultures' prey-finding behavior. Individuals search to explore the potential solution space and move towards better solutions. This process is combined with a competitive selection mechanism to determine the best solutions among individuals.

The AVO algorithm has demonstrated its effectiveness in solving various optimization problems, as evidenced by several studies [15], [17-25]. It has been successfully applied to complex real-world problems inspired by nature, as well as function optimization, data mining, machine learning, artificial neural networks, and other domains [15]. AVO offers several key advantages, including computational efficiency, the ability to perform global searches, scalability, and high solution accuracy. This section provides a summary of the general steps of the African Vultures Optimization (AVO) algorithm. For more comprehensive details and in-depth explanations, readers are encouraged to refer to [15]. This optimization is capable of resolving major optimization issues and has a low computational complexity of O(P X (M + Mb). Here, 'P' stands for population size, 'M' for the maximum number of iterations, and 'b' for the dimensions of the problem.

The behavior of vultures in nature while foraging is depicted in Fig. 2. When many vultures congregate around one food source, it can cause severe conflicts over food acquisition. At such times, physically powerful vultures prefer not to share food with other vultures, as shown in Fig. 2(a). Vulture rotational motion is modeled using spiral motion in Fig. 2(b). The distance between the vulture and one of the two best vultures is first calculated in this method. Moreover, a spiral between the vulture and one of the best vultures is created. As seen in Fig. 2(c), when vultures are hungry and have low energy, vulture gathers together in search of food. Vultures compete in this pursuit. Vultures are aggressive in this search.

In general, the steps of the algorithm are as follows.

Step 1.

Create the initial population by considering the fitness function.

Step 2.

Choose the two best solutions as the best vultures of the first group and the second-best solution as the best vultures of the second group.

Step 3.

Move the other vultures to the best vultures using equations 9 and 10.

$$E(i) = \begin{cases} \text{Vulture}_{Best1} \;\; if \;\; k_i = \beta_1 \\ \text{Vulture}_{Best2} \;\; if \;\; k_i = \beta_2 \end{cases} \quad (9)$$

In Eq. (9), $\text{Vulture}_{\text{Best1}}$ represents the position vector of the best vulture in the first group in the current iteration, and $\text{Vulture}_{\text{Best2}}$ represents the position vector of the best vulture in the second group. One of the top vultures in the current iteration is represented by the position vector E(i). This vector is selected based on the given selection operator in Eq. (10). β_1 and β_2 are parameters measured before the search process. The values of these parameters range between zero and one, and the sum of both parameters is equal to one.

$$k_i = \frac{F_i}{\sum_{i=1}^{n} F_i} \quad (10)$$

Step 4.

Use equations (11) and (12) to search for food.

$$F = (2 \times rand_1 + 1) \times m_1 \times \left(1 - \frac{\text{it}_i}{\max_{\text{it}}}\right) + t \quad (11)$$

$$t = m_2 \times \left(\sin^{m_3}\left(\frac{\pi}{2} \times \frac{\text{it}_i}{\max_{\text{it}}}\right) + \cos\left(\frac{\pi}{2} \times \frac{\text{it}_i}{\max_{\text{it}}}\right) - 1\right) \quad (12)$$

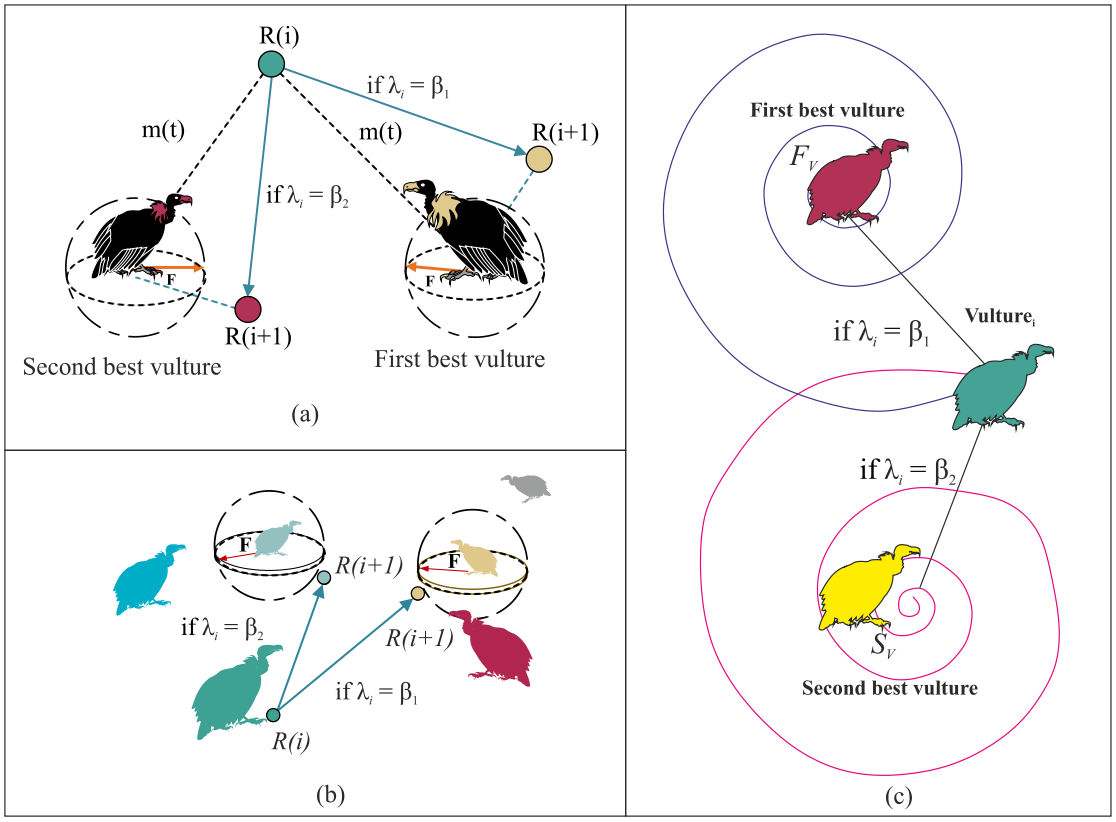

Fig.2. Natural behavior of vultures while foraging a) competition for food, b) rotating flight of vultures, c) aggressive competition for Food.

The F value given in Eq. (11) shows the saturation rate of vultures. it_i represents the valid number of iterations, max_{it} represents the maximum number of iterations. The rand1, m_1, m_2 parameters take random values in the ranges [0,1], [-1,1] and [2,-2], respectively. The m_3 parameter is a constant number. Increasing this value increases the probability of entering the exploration phase towards the maximum iteration.

|F| If the value is greater than or equal to 1, the exploration phase begins, and the vultures forage for the best vulture location at random locations. In order to benefit from different exploration strategies, the k_1, and $rand_{k1}$ parameters, which take random values in the [0,1] range, are compared. Eqs. 13 and 14 are used if k_1 is greater than or equal to randk1. If k1 is less than randk1, Eq.15 is used.

$$K(i+1) = E(i) - D(i) \times F \tag{13}$$

$$D(i) = |\, 2 \times rand_2 \times E(i) - K(i) \,| \tag{14}$$

$$K(i+1) = E(i) - F + rand_3 \times \left((s_2 - s_1) \times rand_d + s_1 \right) \tag{15}$$

In equation, K(i) refers to the vulture's current position vector, and K(i+1) is the position vector in the following iteration. The lower and upper limits of the search space are represented by s_1 and s_2, respectively. The parameters $rand_2$, $rand_3$, and $rand_4$ are assigned a random value between 0 and 1.

$$K(i+1) = D(i) \times \left(F + rand_4 \right) - m(t) \tag{16}$$

$$m(t) = E(i) - K(i) \tag{17}$$

$$K(i+1) = E(i) - \left(S_1 + S_2 \right) \tag{18}$$

$$\begin{aligned} S_1 &= E(i) \times \left(\frac{rand_5 \times K(i)}{2\pi} \right) \times \cos(K(i)) \\ S_2 &= E(i) \times \left(\frac{rand_6 \times K(i)}{2\pi} \right) \times \sin(K(i)) \end{aligned} \tag{19}$$

|F| when the value is less than 0.5, the k_3 and $rand_{k3}$ parameters are compared. If k_3 is equal to or greater than $rand_{k3}$, when using Eq.20 and Eq.21; If k_3 is less than $rand_{k3}$, 21 and 22 are used in the equation. Thus, the accumulation and aggressive bickering of vultures around the food source is modeled.

$$K(i+1) = \frac{B_1 + B_2}{2} \tag{20}$$

$$\begin{aligned} B_1 &= \text{Vulture}_{Best1}(i) - \frac{\text{Vulture}_{Best1}(i) \times K(i)}{\text{Vulture}_{Best1}(i) - K(i)^2} \times F \\ B_2 &= \text{Vulture}_{Best2}(i) - \frac{\text{Vulture}_{Best2}(i) \times K(i)}{\text{Vulture}_{Best2}(i) - K(i)^2} \times F \end{aligned} \tag{21}$$

$$K(i+1) = E(i) - |\, d(t) \,| \times F \times Levy(d) \tag{22}$$

$$L(z) = 0.01 \times \frac{m_4 \times \sigma}{|m_5|^{\frac{1}{\lambda}}},$$

$$\sigma = \left(\frac{\Gamma(1+\lambda) \times \sin\left(\frac{\pi\lambda}{2}\right)}{\Gamma(1+\lambda) \times \lambda \times 2^{\left(\frac{\lambda-1}{2}\right)}} \right)^{\frac{1}{\lambda}} \quad (23)$$

In Eq. (23) λ is a constant number, parameters m_4 and m_5 take random values between 0 and 1. $\Gamma(z) = (z-1)!$. The flow chart of AVOA is given in Fig. 3.

D. Application of AVO Algorithm to SHE-PMW equations

The AVO algorithm implemented in MATLAB was utilized to solve the SHE equations (5), and (6) for the targeted harmonics in the 7, and 11-level inverters, respectively. Three scenarios were considered, with a population size of 100 and 100 iterations. The solutions were obtained by incrementing the modulation index M from 0 to 1 in steps of 0.01. The calculations were performed on a personal computer equipped with an Intel(R) Core (TM) i7-10870H CPU @ 2.20GHz, 16.0 GB RAM, and a GeForce RTX 2060 NVIDIA graphics card. At each step, the obtained solution was evaluated using a fitness function. The objective was to determine the switching angles that either eliminate or reduce the selected low-order harmonics to an acceptable level while achieving the desired voltage value. Eq. (24) defines the fitness function used for each set of solutions. The goal of this optimization process was to find the optimal set of switching angles that minimizes the distortion caused by the harmonics, ensuring the output voltage closely matches the desired waveform. The AVO algorithm, with its population-based approach and imitation of vulture behavior, efficiently searched the solution space to find the best configuration of switching angles for each modulation index.

$$f = \min_{\theta_i} \left\{ \left| V_{ref} - V_{1p} \right| + \left(\frac{4V_{DA}}{n\pi} . \left(\sum_{i=2}^{k} \cos(n\theta_i) \right) \right)^2 \right\} = 0 \quad (24)$$

In Eq. (24) V_{ref} represents the maximum value of the desired base voltage, while V_{1p} represents the maximum value of the base voltage obtained at the inverter output applying the calculated switching angles to the inverter. The fundamental frequency of the fundamental voltage is 50Hz. Total source voltage values are selected to be a maximum of 311 volts. For the seven-level inverter, all sources are 311/3 volts, and all sources for the eleven-level inverter are 311/5 volts. An RL load was used as the load for both seven-level, and eleven-level CHB-MLI. The value of the resistance R is 10 ohms, and the value of the inductance L is 5 mH. The load connected to the inverter output affects the harmonic formation [26]. Here, harmonic analysis has been made only for RL load. The simulation results are explained in the next section.

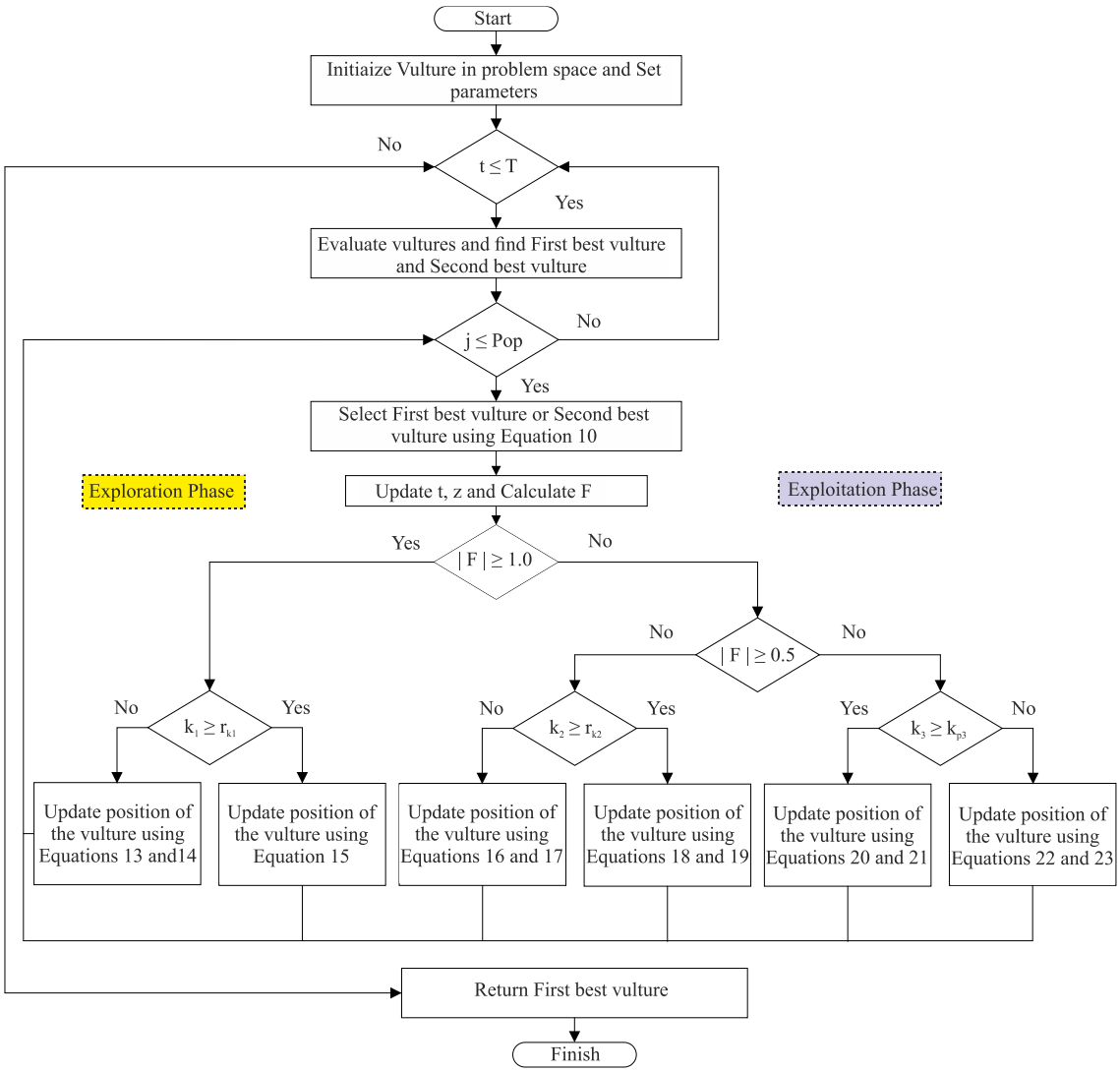

Fig.3. AVOA [15]

III. Results And Discussion

To assess the effectiveness of the AVOA optimization in solving the SHE-PWM equations, the results obtained from applying the AVOA algorithm in the MATLAB Simulink environment for the 7-, and 11-level inverters are discussed below.

TABLE I
PARAMETER SETTING OF AVOA

Parameter	Value
β_1	0.8
β_2	0.2
w	2.5
k_1	0.6
k_2	0.4
k_3	0.6

Table I displays the parameters utilized for AVOA at levels 7 and 11. The w operator mentioned in Table II is a parameter that influences the extent of disruption during the exploration and exploitation phases.

A. *Simulation results for seven-level MLI*

The graph in Fig. 4(a) depicts the fitness function values for each set of switching angles across the range of modulation index values Fig. 4(b) displays the switching angles determined for the corresponding modulation index values, providing insight into the optimal configuration for the 7-level MLI. In Fig. 4(c), the plots showcase the THD, THDe, and magnitudes of the 5^{th} and 7^{th} harmonics. These metrics are evaluated for modulation index values, highlighting the system's harmonic performance. Notably, the graph indicates that solutions within the M range of 0.1 to 0.4 fail to meet the IEEE-519 standard [27], while acceptable solutions are found in the M range of 0.5 to 1.0.

The switching angles calculated by AVO versus different modulation indices for 7-level MLI are shown in Table II. The switching angles calculated in Table II were applied to the 7-

level inverter in the Matlab environment, and the simulation output values are shown in Table III.

As shown in Table III, the AVO algorithm has successfully found suitable solutions for the 7-level inverter within the modulation index range of 0.1 to 1.0. The desired fundamental voltage is controlled with an error of less than 0.5% compared to the reference value. The 0.5 to 1.0 index values modulation range effectively suppresses the selected harmonics. Examining this range, both the THDe value and the magnitudes of the 5th and 7th harmonics are below 0.09%. Figure 5 illustrates the load voltage waveforms for modulation indices of 0.4, 0.6, and 1.0. The THD and THDe analysis of these waveforms is presented in Figure 6 and Figure 7, respectively.

For a modulation index of M=0.4, the voltage waveform of the load exhibits a THD value of 16.94%. The maximum value of the fundamental voltage, Van(max), is measured as 124.2V, and the rms value, Van(rms), is calculated as 87.83V (Figure 6(a)). For a modulation index of M=0.6, the THD of the load voltage waveform is determined as 12.41%. The maximum value of the fundamental voltage, Van(max), is found to be 186.2V, and the rms value, Van(rms), is calculated as 131.7V (Figure 6(b)). Finally, for a modulation index of M=1.0, the THD of the load voltage waveform is reduced to 7.83%. The maximum value of the fundamental voltage, Van(max), is measured as 311.1V, and the rms value, Van(rms), is determined as 220.1V (Figure 6(c)).

Figure 7 illustrates the extent to which the selected harmonics are eliminated. For M=0.4 modulation index, the calculated values are THDe=%6.35, h5=%3.99 (V5=4.95V), and h7=%3.99 (V7=6.14V). For M=0.6 modulation index, the calculated values are THDe=%0.09, h5=%0.02 (V5=0.03V), and h7=%0.15 (V7=0.08V). Lastly, for M=1.0 modulation index, the calculated values are THDe=%0.04, h5=%0.03 (V5=0.01V), and h7=%0.01 (V7=0.03V).

The analysis indicates that the AVO algorithm precisely controls the fundamental voltage and effectively suppresses the selected harmonics within the modulation index range of 0.5 to 1.0. The obtained results demonstrate the capability of the AVO algorithm to achieve desired voltage control and harmonic suppression for the 7-level inverter.

B. Simulation results for eleven-level MLI

The graph in Fig. 8(a) depicts the fitness function values for each set of switching angles across the range of modulation index values Fig. 8(b) displays the switching angles determined for the corresponding modulation index values, providing insight into the optimal configuration for the 11-level MLI. In Fig. 8(c), the plots showcase the THD, THDe, and magnitudes of the 5th, 7th,11th and 13th harmonics. These metrics are evaluated for modulation index values, highlighting the system's harmonic performance. Notably, the graph indicates that solutions within the M range of 0.1 to 0.4 fail to meet the IEEE-519 standard, while acceptable solutions are found in the M range of 0.5 to 1.0.

The switching angles calculated by AVO versus different modulation indices for 11-level MLI are shown in Table IV. The switching angles calculated in Table IV were applied to the 11-level inverter in the Matlab environment, and the simulation output values are shown in Table V.

TABLE II
SWITCHING ANGLES CALCULATED WITH AVO (FOR 7 LEVELS)

Modulation Index	**Switching Angles (Radians)**		
M	**θ_1**	**θ_2**	**θ_3**
0.1	1.3329	1.5708	1.5708
0.2	1.0801	1.5708	1.5708
0.3	0.8907	1.4928	1.5708
0.4	0.7787	1.3380	1.5708
0.5	0.7115	1.1488	1.5597
0.6	0.6882	1.0224	1.4504
0.7	0.6691	0.9414	1.2908
0.8	0.5102	0.9503	1.1254
0.9	0.3056	0.7512	1.1196
1.0	0.2029	0.5370	1.0181

TABLE III
SIMULATION RESULTS (FOR 7 LEVELS)

M	Vref(peak)	V_{ref}(rms)	V(rms)	Error (%)	THD (%)	THD_e (%)	h_5	h_7
0.10	31.1	22	21.96	**0.18**	109.14	99.42	79.03	60.32
0.20	62.2	44	43.95	**0.11**	37.77	28.44	27.09	8.68
0.30	93.3	66	65.83	**0.26**	32.95	10.37	3.65	9.71
0.40	124.4	88	87.83	**0.19**	16.94	6.35	3.95	4.95
0.50	155.5	110	109.8	**0.18**	17.44	**0.06**	**0.01**	**0.06**
0.60	186.6	132	131.7	**0.23**	12.41	**0.09**	**0.02**	**0.08**
0.70	217.7	154	153.6	**0.26**	12.26	**0.07**	**0.02**	**0.06**
0.80	248.8	176	175.6	**0.23**	10.72	**0.04**	**0.01**	**0.00**
0.90	279.9	198	197.4	**0.30**	11.81	**0.03**	**0.00**	**0.01**
1.00	311.0	220	220.1	**0.05**	7.84	**0.04**	**0.01**	**0.03**

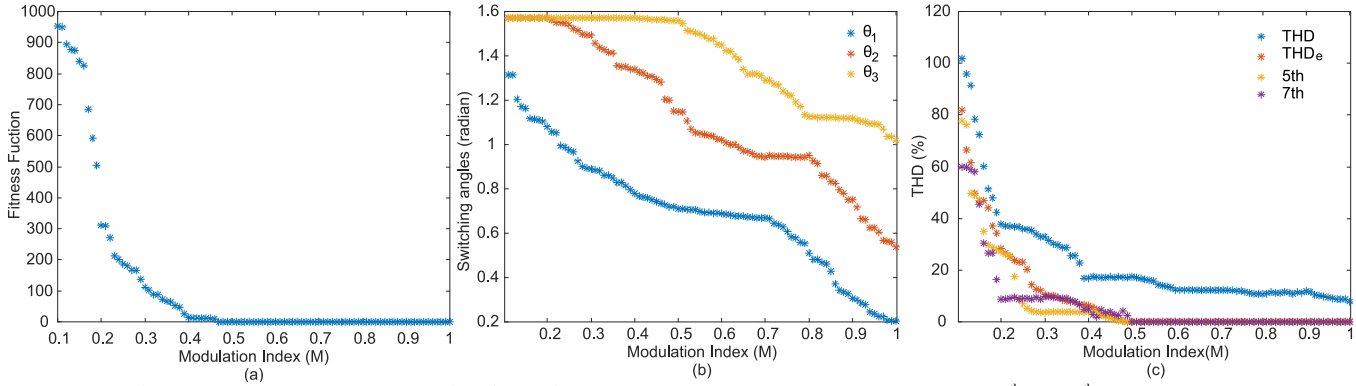

Fig.4. Analysis of the 7-level MLI inverter in terms of (a) fitness function, (b) switching angles, and (c) THD, THDe, 5th , and 7th harmonic characteristics as a function of M.

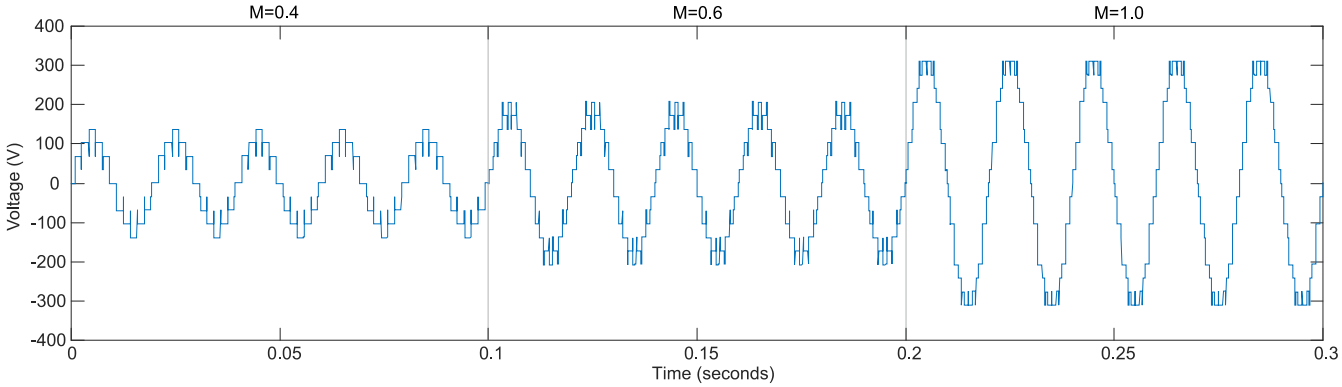

Fig.5. Load voltage waveforms for different modulation indices (7-level): (a) M=0.4, (b) M=0.6, (c) M=1.0

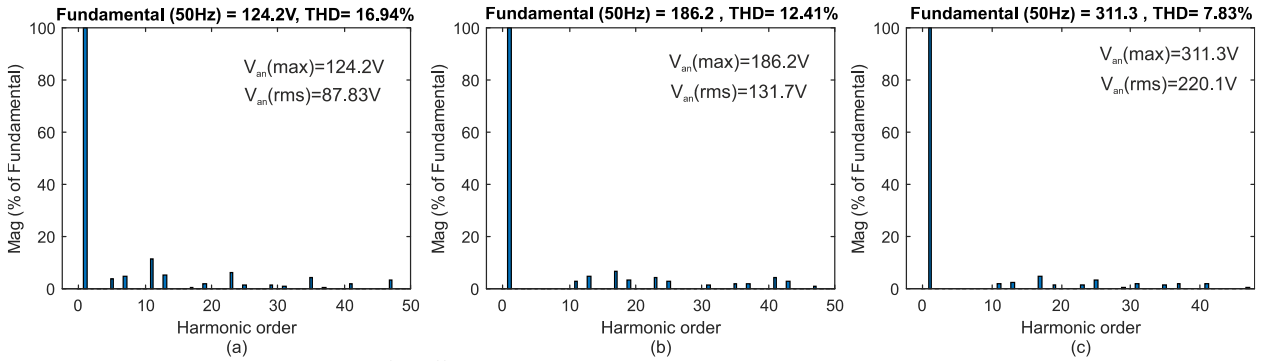

Fig.6. THD values for different modulation indices (7-level) (a) M=0.4, (b) M=0.6, (c) M=1.0

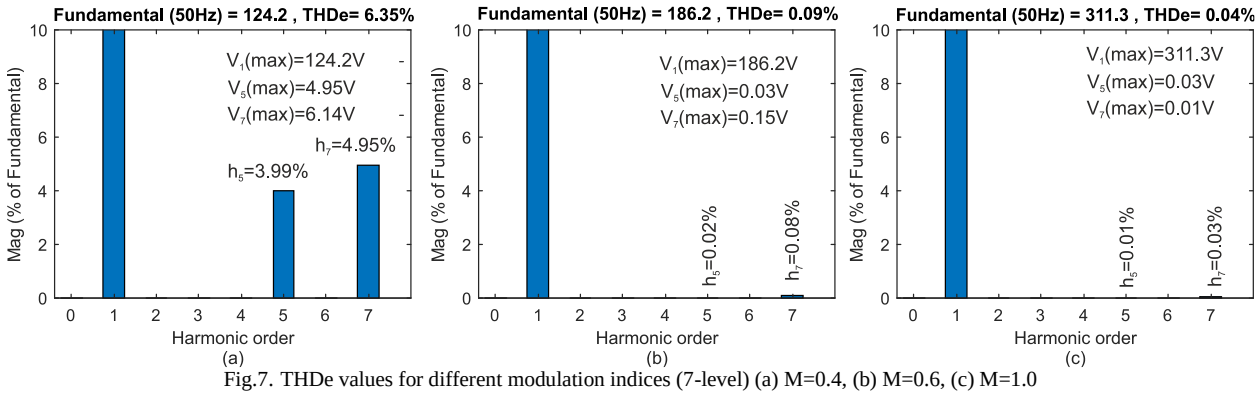

Fig.7. THDe values for different modulation indices (7-level) (a) M=0.4, (b) M=0.6, (c) M=1.0

TABLE IV
SWITCHING ANGLES CALCULATED WITH AVO (FOR 11 LEVELS)

Modulation Index	**Switching Angles (Radians)**				
M	**θ_1**	**θ_2**	**θ_3**	**θ_4**	**θ_5**
0.1	1.1672	1.5708	1.5708	1.5708	1.5708
0.2	0.7575	1.5119	1.5708	1.5708	1.5708
0.3	0.7706	1.1356	1.5317	1.5708	1.5708
0.4	0.6859	0.9827	1.3266	1.5704	1.5708
0.5	0.6409	0.8684	1.1454	1.4738	1.5708
0.6	0.6168	0.8196	1.0224	1.2672	1.5331
0.7	0.3426	0.6797	0.9852	1.1093	1.5395
0.8	0.3898	0.6855	0.9197	1.0352	1.2386
0.9	0.1334	0.4805	0.7115	0.9169	1.2745
1.0	0.1332	0.3363	0.5102	0.8244	1.1008

TABLE V
SIMULATION RESULTS (FOR 11 LEVELS)

M	**Vref(peak)**	**Vref(rms)**	**V(rms)**	**Error (%)**	**THD (%)**	**THDe (%)**	**h_5**	**h_7**	**h_{11}**	**h_{13}**
0.10	31.1	22	21.91	**0.41**	59.35	55.17	46.09	11.48	0.31	17.01
0.20	62.2	44	43.84	**0.36**	27.64	18.27	12.34	2.88	12.38	2.19
0.30	93.3	66	65.74	**0.39**	19.34	8.12	4.32	3.26	0.01	6.06
0.40	124.4	88	87.66	**0.39**	12.77	3.10	2.32	0.71	1.89	0.39
0.50	155.5	110	109.2	**0.73**	9.05	**0.95**	**0.47**	**0.25**	**0.70**	**0.34**
0.60	186.6	132	131.5	**0.38**	6.48	**0.09**	**0.05**	**0.04**	**0.02**	**0.02**
0.70	217.7	154	153.3	**0.45**	8.10	**0.05**	**0.02**	**0.02**	**0.03**	**0.01**
0.80	248.8	176	175.2	**0.45**	6.72	**0.03**	**0.01**	**0.00**	**0.02**	**0.01**
0.90	279.9	198	197.2	**0.40**	6.31	**0.05**	**0.02**	**0.00**	**0.01**	**0.02**
1.00	311.0	220	219.8	**0.09**	4.49	**0.03**	**0.02**	**0.01**	**0.01**	**0.01**

As shown in Table V, the AVO algorithm has successfully found suitable solutions for the 11-level inverter within the M range of 0.1 to 1.0. It is observed that the desired fundamental voltage is controlled with an error of less than 0.5% compared to the reference value. M range of 0.6 to 1.0 is identified as the effective range for suppressing selected harmonics. Within this range, both the THDe load value and the magnitudes of the 5th, 7th, 11th, and 13th harmonics are below 0.09%.

In Fig. 9, the voltage waveforms of the load are shown for modulation indices of 0.4, 0.6, and 1.0. The THD and THDe analyses of the waveforms are presented in Figures 10 and 11, respectively. For a modulation index of 0.4, the THD of the load voltage is calculated to be 12.27%, with a maximum value of Van(max) = 124V and an RMS value of Van(rms) = 87.71V (Fig. 10(a)). For a modulation index of 0.6, the THD of the load voltage is calculated to be 6.84%, with a maximum value of Van(max) = 185.9V and an RMS value of Van(rms) = 131.5V (Fig. 10(b)). Finally, for a modulation index of 1.0, the THD of the load voltage is determined to be 4.48%, with a maximum value of Van(max) = 310.8V and an RMS value of Van(rms) = 219.8V (Fig. 10(c)).

The degree of suppression of the selected harmonics is shown in Fig. 11. For a modulation index of 0.4, the THDe is calculated to be 3.10%, with harmonic magnitudes of $h_5 = 2.32$ ($V_5 = 2.88$V), $h_7 = 0.71$ ($V_7 = 0.89$V), h11 = 1.89 ($V_{11} = 2.34$V), and $h_{13} = 1.89$ ($V_{13} = 2.34$V). For a modulation index of 0.6, the THDe is determined to be 0.09%, with harmonic magnitudes of h5 = 0.05 ($V_5 = 0.08$V), $h_7 = 0.04$ (V7 = 0.07V), $h_{11} = 0.02$ (V_{11}

= 0.04V), and h_{13} = 0.02 (V_{13} = 0.03V). Finally, for a modulation index of 1.0, the THDe is found to be 0.04%, with harmonic magnitudes of h5 = 0.02 (V_5 = 0.05V), h_7 = 0.01 (V_7 = 0.03V), h_{11} = 0.01 (V_{11} = 0.02V), and h_{13} = 0.01 (V_{13} = 0.04V).

IV. Conclusion

This study utilized the recently developed AVOA (Artificial Virus Optimization Algorithm) to tackle the SHE-PWM (Selective Harmonic Elimination Pulse Width Modulation) issue in multilevel inverters. The effectiveness of AVOA in resolving SHE-PWM was showcased through MATLAB simulations conducted on 7 and 11 level cascade H-bridge inverters. The algorithm has demonstrated its capability to find suitable solutions within the M range of 0.1 to 1.0. The desired reference voltage has been effectively controlled with an error of less than 0.5%. Furthermore, the selected harmonics have been efficiently suppressed within the modulation range of 0.6 to 1.0, as indicated by the THDe values and the magnitudes of the 5th, 7th , 11th , and 13th harmonics, all of which are below 0.09%.

The waveform analysis of the output voltage for different modulation indices (0.4, 0.6, and 1.0) has shown that the THD values decrease as the modulation index increases. The maximum values of the fundamental voltage and its RMS value have also been determined for each modulation index, providing important insights into the performance of the system. Overall, the AVO algorithm has proven its effectiveness in achieving accurate voltage control and harmonic suppression in multilevel inverters, thereby contributing to the improvement of power quality and efficient operation of the system.

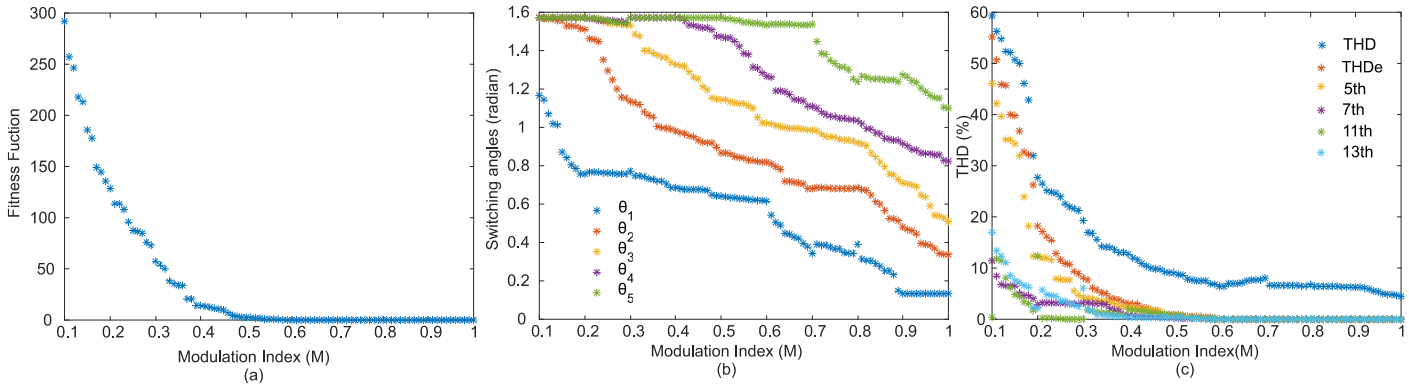

Fig.8. Analysis of the 11-level MLI inverter in terms of (a) fitness function, (b) switching angles, and (c) THD, THDe, 5th , 7th, 11th and 13th harmonic characteristics as a function of M.

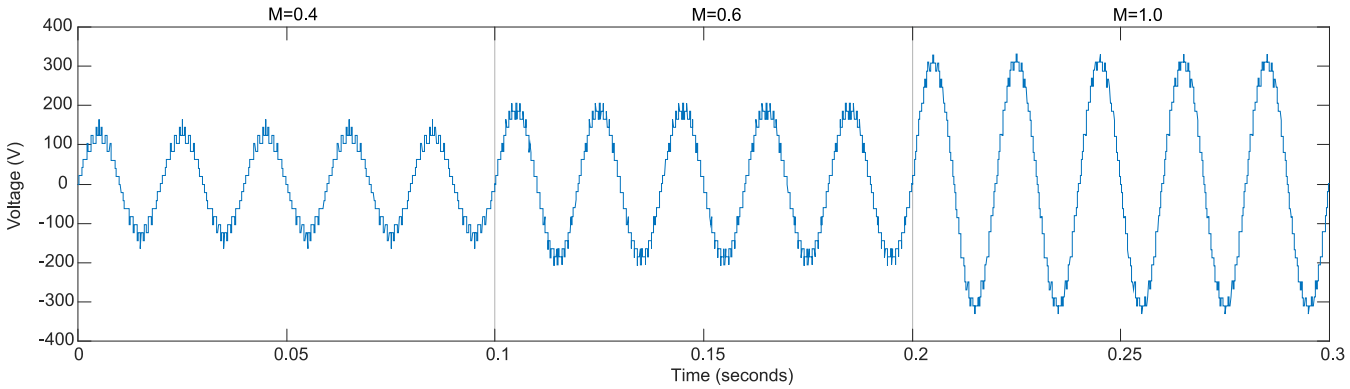

Fig.9. Load voltage waveforms for different modulation indices (11-level) (a) M=0.4, (b) M=0.6, (c) M=1.0

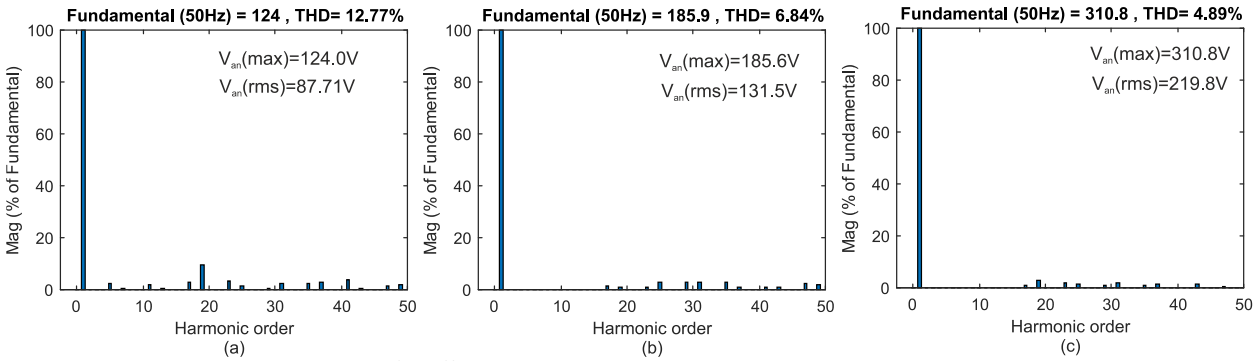

Fig.10. THD values for different modulation indices (11-level) (a) M=0.4, (b) M=0.6, (c) M=1.0

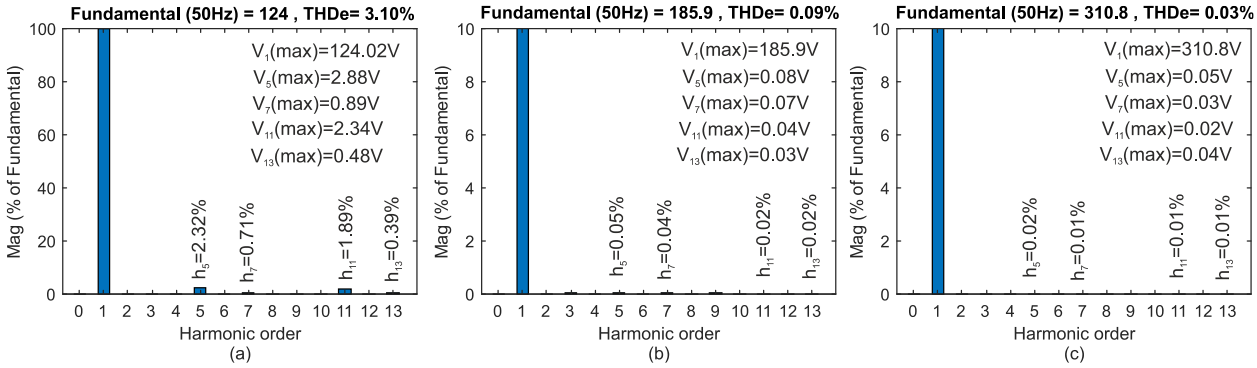

Fig.11. THDe values for different modulation indices (11-level) (a) M=0.4, (b) M=0.6, (c) M=1.0

REFERENCES

[1] A. Raki, Y. Neyshabouri, M. Aslanian, & H. Iman-Eini, "A Fault-Tolerant Strategy for Safe Operation of Cascaded H-Bridge Multilevel Inverter under Faulty Condition". IEEE Transactions on Power Electronics.

[2] B. Karthikeyan, B. Swetha, C. Shahana, B. Vijay, & M. Swathi, "Switched Capacitor Based Multilevel Inverter for\newline PV System". In 2023 9th International Conference on Electrical Energy Systems (ICEES) (pp. 471-475). IEEE. March, 2023.

[3] N. Padmamalini, P. Deepa, T. Joel, S. Loganayagi, M. F. Banu, & S. Gomathi, "Control of Diode Clamped Multilevel Inverter based STATCOM for Reactive Power Compensation using H-bridge Topology". In 2023 7th International Conference on Intelligent Computing and Control Systems (ICICCS) (pp. 1860-1865). IEEE.

[4] H. I. Hazim, K. A. Baharin, C. K. Gan, A. H. Sabry, & A. J. Humaidi, Review on optimization techniques of PV/inverter ratio for grid-Tie PV systems. Applied Sciences, 13(5), 3155, 2023.

[5] C. Mayet, D. Labrousse, R. Bkekri, F. Roy, & G. Pongnot, "Energetic Macroscopic Representation and Inversion-Based Control of a Multi-Level Inverter with Integrated Battery for Electric Vehicles". In 2021 IEEE Vehicle Power and Propulsion Conference (VPPC) (pp. 1-6). IEEE, October, 2021.

[6] C. Pisani, G. Bruno, H. Saad, P. Rault, & B. Clerc, "Functional validation of a real VSC HVDC control system in black start operation", In 2019 AEIT HVDC International Conference (AEIT HVDC) (pp. 1-6). IEEE. May, 2019.

[7] H. Lin, R. Chen, R. Li, L. Zhu, H. Yan, & Z. Shu , "A flexible and fast space vector pulse width modulation technique for multilevel converters", In 2019 22nd International Conference on Electrical Machines and Systems (ICEMS) (pp. 1-4). IEEE, August, 2019.

[8] S. A. Azmi, A. A. Shukor, & S. R. A. Rahim, "Performance evaluation of single-phase H-bridge inverter using selective harmonic elimination and sinusoidal PWM techniques", In 2018 IEEE 7th International Conference on Power and Energy (PECon) (pp. 67-72). IEEE, December, 2018.

[9] S. E. Arslan, F. E. Uzun, K. Gürkan, A. Acar, İ. O. Yildirim, , U. Güven, ... & S. Yarman, "Realization of SV-PWM motor control algorithm using ARM Cortex-M4 based microcontroller", In 2016 National Conference on Electrical, Electronics and Biomedical Engineering (ELECO) (pp. 282-285). IEEE. December, 2016.

[10] E. Bektas, & H. Karaca, "GA based selective harmonic elimination for multilevel inverter with reduced number of switches: an experimental study", Elektronika ir Elektrotechnika, 25(3), 10-17, 2019.

[11] A. Pourdadashnia, M. Farhadi-Kangarlu, B. Tousi, & M. Sadoughi ,. "SHM-PWM technique in a cascaded H-bridge multilevel inverter with adjustable DC-link for wide voltage range applications", International Journal of Circuit Theory and Applications, 51(5), 2228-2246, 2023.

[12] S. Pani, N. Guru, D. Puhan, & A. K. Barisal, "Comparative Performance analysis of Multilevel Inverter through meta heuristics", In 2022 6th International Conference on Intelligent Computing and Control Systems (ICICCS) (pp. 129-135). IEEE, May, 2022.

[13] B. G. Babu & M. S. Kalavathi, "Hardware Implementation of Multilevel Inverter using NR, GA, Bee Algorithms" In 2021 International Conference on Sustainable Energy and Future Electric Transportation (SEFET) (pp. 1-6). IEEE. January, 2021.

[14] Y. Bektaş, & H. Karaca, "Red deer algorithm based selective harmonic elimination for renewable energy application with unequal DC sources" Energy Reports, 8, 588-596, 2022.

[15] B. Abdollahzadeh, F. S. Gharehchopogh, & S. Mirjalili, African vultures optimization algorithm: A new nature-inspired metaheuristic algorithm for global optimization problems", Computers & Industrial Engineering, 158, 107408, 2021.

[16] H. Karaca, & E. Bektas, "Selective Harmonic Elimination Technique Based on Genetic Algorithm for Multilevel Inverters", In Transactions on Engineering Technologies: World Congress on Engineering and Computer Science 2015 (pp. 333-347). Springer Singapore, 2017

[17] M. YEŞİLBUDAK, "Extraction of photovoltaic cell and photovoltaic module parameters using african vultures optimization algorithm" Gazi University Journal of Science Part C: Design and Technology, 9(4), 708-725.

[18] M. E. Bento, "Design of a Resilient Wide-Area Damping Controller Using African Vultures Optimization Algorithm", In 2021 31st Australasian Universities Power Engineering Conference (AUPEC) (pp. 1-6). IEEE, September ,2021.

[19] H. E. ALOUACHE, S. SAYAH, & A. HAMOUDA, "Africa vultures optimization algorithm for optimal power flow solution including SVC devices", In 2022 19th International Multi-Conference on Systems, Signals & Devices (SSD). IEEE. May, 2022

[20] R. Liu, T. Wang, J. Zhou, X. Hao, Y. Xu, & J. Qiu, "Improved African vulture optimization algorithm based on quasi-oppositional differential evolution operator", IEEE Access, 10, 95197-95218, 2022.
[21] D. Gürses, P. Mehta, S. M. Sait, & A. R. Yildiz, African vultures optimization algorithm for optimization of shell and tube heat exchangers", Materials Testing, 64(8), 1234-1241. 2022.
[22] J. Zhang, M. Khayatnezhad, & N. Ghadimi, "Optimal model evaluation of the proton-exchange membrane fuel cells based on deep learning and modified African Vulture Optimization Algorithm". Energy Sources, Part A: Recovery, Utilization, and Environmental Effects, 44(1), 287-305. 2022.
[23] M. Ahmed, M. Khamies, G. Magdy, & S. Kamel, "Designing Optimal PI λ D μ Controller for LFC of Two-Area Power Systems Using African Vulture's Optimization Algorithm", In 2021 22nd International Middle East Power Systems Conference (MEPCON) (pp. 430-437). IEEE, December, 2021.
[24] S. Mil'shtein, & D. N. Asthana, "Brief Comparison of Tandem and Cascaded Solar Cells", In 2021 IEEE 48th Photovoltaic Specialists Conference (PVSC) (pp. 2260-2263). IEEE, June, 2021.
[25] F. S. Gharehchopogh, "An improved Harris Hawks optimization algorithm with multi-strategy for community detection in social network" Journal of Bionic Engineering, 20(3), 1175-1197, 2023.
[26] T. Sonmezocak, O. Akar, & U. K. Terzi, "HIGH PERFORMANCE ADAPTIVE ACTIVE HARMONIC FILTER DESIGN FOR NON-LINEAR LED LOADS" Light & Engineering, 30(1), 29-38, 2022.
[27] A. Demirci, O. Akar, U. K. Terzi, & T. Sönmezocak, "Investigation of International Harmonic Standards in Power Systems", In 4th International Mardin Artuklu Scientific Research Congress (pp. 7-8), 2020, August.